A Novel Hybrid Dual-PM Machine Excited by AC with DC Bias for Electric Vehicle Propulsion

Qingsong Wang, Shuangxia Niu, *Member, IEEE* and Xiang Luo, *Member, IEEE*

***Abstract*—This paper proposes a novel hybrid-excited dual-PM machine for electric vehicle propulsion. The key is to use an integrated stator winding to replace the armature winding and the field winding in conventional hybrid-excited machine. The stator winding is excited by AC current with DC bias, in which the AC component is used to produce the rotating armature field, while the DC bias current is used for flux regulation. Therefore, the function of the AC and DC windings can be incorporated and realized by using just one set of winding. The torque density and flux regulating capability can be improved, and the winding configuration is also simplified. In addition, dual-PM excitation structure combines the advantage of stator-PM doubly salient machine and rotor-PM magnetic geared machine, which can further enhance the torque capability. The operating principle and control strategy of the proposed machine are discussed. The electromagnetic performances are studied using time-stepping finite element method (TS-FEM). A machine prototype is manufactured and experimental tests are conducted to verify the effectiveness of the machine design.**

***Index Terms*—DC bias, dual-PM, flux regulation, hybrid-excited machine.**

I. INTRODUCTION

DUE to the increasing concerns on energy crisis and environmental pollution, electric vehicles (EVs) have attracted much attention and been widely investigated by researchers for their theoretical zero emission [1-6]. Usually the driving motor for EV propulsion should have the following features: 1) High torque density to provide enough driving force during start-up, climbing and accelerating; 2) High efficiency to increase the driving distance; 3) Good flux regulating capability to widen the constant power speed range.

Permanent magnet (PM) machines are promising candidates for EV propulsion [7-9], for their inherent high torque density and high efficiency. In direct-drive PM machines, since additional gear box based transmission mechanism is eliminated, simplified structure and improved efficiency can be achieved. In recent years, a relatively new class of PM machines with flux modulating capability is proposed [10-17]. This kind of machine usually has high torque density due to the magnetic gearing effect, and flexible pole-slot combination, which is especially suitable for low-speed direct-drive applications. Nevertheless, it is not easy to regulate the air-gap field due to the their fixed PM excitation. Generally, flux weakening operation is realized via negative d-axis current or advanced conduction angle control, which reduce the output torque at the flux weakening region[18].

Hybrid-excited machines (HEMs) are proposed to deal with the aforementioned problems. The air-gap field can be directly regulated via the DC current in the field winding. Good flux regulating capability can be achieved and position sensor is not necessary for the flux control. A consequent-pole HEM with PM excitation in the rotor and field coils in the stator is proposed in [19]. The air-gap field can be effectively regulated by applying DC current in the field coils without the demagnetization risk for the PM pieces. However, the torque density is reduced as the air-gap associated with the DC winding section does not participate in the torque transmission. Hybrid-excited doubly salient machines (HE-DSMs) with both PMs and field coils located in the stator are widely investigated in [20-25]. The magnetic bridges in [23, 24] and air bridges in [21] are introduced as low reluctance paths for the flux regulation, and hence effectively reduce the required field exciting ampere-turns. Hybrid-excited flux switching machines (HE-FSMs) are also extensively studied in [26-31]. By shortening the length of PMs in original FSPM machines, additional place is saved to house the field windings. The PMs can be located in the top or bottom or middle of the stator slots [30]. Both HE-DSMs and HE-FSMs with rotor merely made up of salient poles, have very robust rotor structure and particularly suitable for high speed applications. Generally, to achieve flux regulation, an additional field winding should be employed in HEM. However, because the field winding just used for flux regulation, and takes up additional slot space, the effective slot area housing the armature winding is reduced when the total slot area is fixed. Consequently, additional field winding reduces the slot space utilization ratio and results in the reduction of torque density, especially when rotating speed is

Manuscript received January 31, 2016; revised April 18, 2016, June 21, 2016, November 3, 2016, December 25, 2016, and February 23, 2017; accepted March 2, 2017. This work was supported by the Research Grant Council, Hong Kong Special Administrative Region, China, under projects PolyU 152130/14E and PolyU 15250916/16E. *(Corresponding author: Shuangxia Niu.)*

Qingsong Wang and Shuangxia Niu are with the Department of Electrical Engineering, The Hong Kong Polytechnic University, Hong Kong (e-mail: q.s.wang@connect.polyu.hk; eesxniu@polyu.edu.hk).

Xiang Luo is with the The Shanghai Jiao Tong University, Shanghai, China(e-mail: maskluo@sjtu.edu.cn).

below the base speed. Meanwhile, the maximum flux regulating range is also restricted by the slot space used for the field coils housing.

This paper presents a novel dual-PM machine excited by AC current with DC bias. Compared with the existing HEM topologies, the proposed machine offers two prominent advantages. One is the dual-PM excitation, which integrates the advantages of stator-PM doubly salient machine and rotor-PM magnetic geared machine. The other is the integrated stator winding excited by AC current with DC bias, which incorporates the function of armature winding and field winding. During constant torque operation, the DC bias current is set to zero, all the current serves as armature current to produce electromagnetic torque, while in constant power region, the DC bias component is added for flux weakening. The AC/DC ratio is adjusted according to speed/ torque requirements. Therefore, the slot space is always fully utilized. For a given current density, the proposed machine has better potential to achieve both high torque density and wide flux regulating range. Meanwhile, the winding configuration is simplified as only one set of winding is used. The operating principle and control strategy are discussed in detail. The electromagnetic performances are studied using time-stepping finite element method (TS-FEM) and verified by experimental tests.

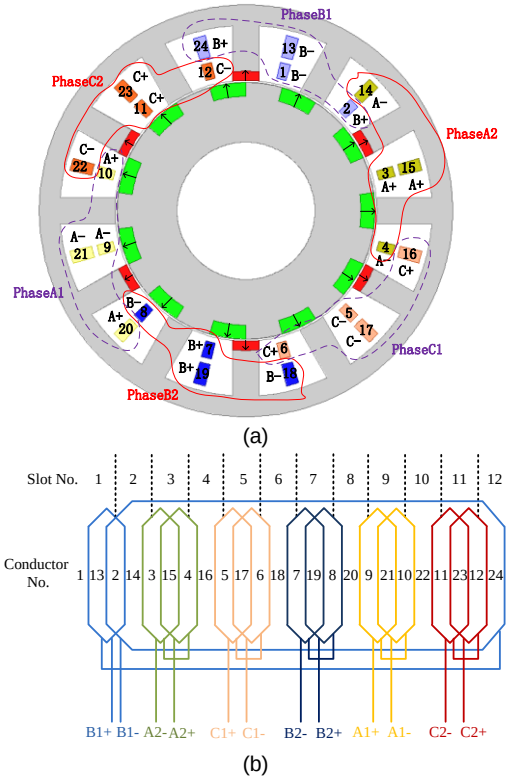

(a)

(b)

Fig. 1. Configuration and winding connection of the proposed machine. (a) Configuration. (b) Winding connection.

II. Configuration And Winding Connection

A. Configuration of the proposed machine

Fig. 1 (a) shows the configuration of the proposed machine, which consists of one rotor and one stator. The PMs are employed on both the rotor and stator, namely dual-PM excitation. All the PMs are radially outward magnetized. Each PM and its adjacent iron tooth form one pair of magnetic poles and dual magnetic-gearing effect can be achieved [32]. The difference in the permeability of the PMs and iron teeth is the key to ensure effective magnetic coupling among the magnetic fields excited by the stator windings and the two sets of PMs.

B. Winding connection

Fig. 1(b) shows the winding connection of the proposed machine. Concentrated coils are employed to reduce the length of end winding, hence to reduce the copper loss and increase the efficiency. The concentrated coils are excited by AC current with DC bias. Each phase is divided into two sub-phases as shown in Fig. 1 (a) and separately controlled. During the flux-weakening operation, sub-phase 1 is excited by 3-phase sinusoidal AC current with positive DC bias, while sub-phase 2 is supplied with sinusoidal AC current with the same amplitude and frequency, but with negative DC bias, as followed.

$$\begin{cases} i_{A1} = I_{ac}\cos\left(2\pi ft\right) + I_{dc} \\ i_{B1} = I_{ac}\cos\left(2\pi ft - 2\pi/3\right) + I_{dc} \\ i_{C1} = I_{ac}\cos\left(2\pi ft - 4\pi/3\right) + I_{dc} \\ i_{A2} = I_{ac}\cos\left(2\pi ft\right) - I_{dc} \\ i_{B2} = I_{ac}\cos\left(2\pi ft - 2\pi/3\right) - I_{dc} \\ i_{C2} = I_{ac}\cos\left(2\pi ft - 4\pi/3\right) - I_{dc} \end{cases} \quad (1)$$

where $i_{A1,\,B1,\,C1}$ and $i_{A2,\,B2,\,C2}$ are the currents of the sub-phase 1 and sub-phase 2, respectively. I_{ac} and f refer to the amplitude and frequency of the sinusoidal AC current, while I_{dc} refers to the DC bias current.

The flux excited by the DC bias current shares the same magnetic path with that of the stator PMs, which enables the DC bias current to achieve flux regulating effectively. Different from negative d-axis current control in conventional vector controlled drives, the flux regulating of the proposed machine is realized via zero-sequence current, which is generated by applying DC bias current in the stator winding. The DC bias current only involves a small voltage drop since the DC reactance is very small. Therefore, the voltage used for generating q-axis current is increased, and the machine can keep a relatively high torque production capability when runs above the base speed.

III. Working Principle

The working principle of the proposed machine is based on the magnetic-gearing effect. Apart from the original fundamental harmonics excited by the PMs and the armature currents, many other field harmonics are generated when modulated by the salient segments in rotor and stator. Harmonics with the same pole-pairs and the same rotating speed will couple together to produce steady electromagnetic torque. The rotor PM pole-pairs p_r, stator PM pole-pairs p_s and armature field pole-pairs p_a are governed by [33]

$$p_r = p_s + p_a \quad (2)$$

The frequency of the armature current f is determined by the rotating speed n and rotor pole-pairs p_r.

$$f = \frac{np_r}{60} \tag{3}$$

The stator slot number N_s is twice the pole-pairs of the stator PMs.

$$N_s = 2p_s \tag{4}$$

As shown in Fig. 1(a), both the stator and rotor have PM excitation. The proposed machine can be regarded as combination of a stator-PM doubly salient machine and a rotor-PM magnetic geared machine.

A. Stator-PM doubly salient machine

If the rotor PMs are removed, a stator-PM doubly salient machine is obtained. The open-circuit field distributions at different rotor angular positions are shown in Fig. 2, where θ_{rotor} refers to the rotor position.

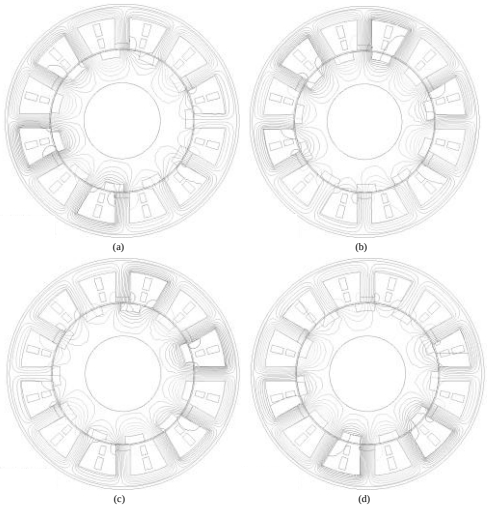

Fig. 2. Open-circuit field distributions at different rotor positions when rotor PMs are removed. (a) $\theta_{rotor} = 0^\circ$. (b) $\theta_{rotor} = 8.18^\circ$.(c) $\theta_{rotor} = 16.36^\circ$. (d) $\theta_{rotor} = 24.54^\circ$.

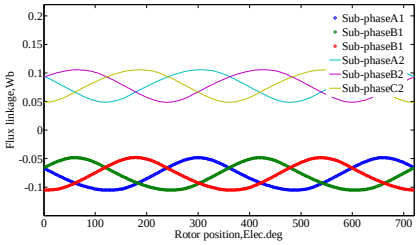

Fig. 3. Flux linkage when rotor PMs are removed.

The stator flux linkage and the back EMF at 800 rpm are given in Fig. 3 and Fig. 4, respectively. One can find that although the PMs in the stator are stationary, sinusoidal flux linkage can be produced due to the variation of magnetic reluctance when the rotor rotates. The flux linkage of each sub-phase is synchronous, and the flux bias components in the two sub-phases have the same magnitude but in opposite direction. Therefore, to regulate the air-gap flux, the DC bias currents in the two sub-phases should also have the opposite polarity, as illustrated in Eq. (1). Balanced EMF waveforms can be obtained as shown in Fig. 4. The EMF waveforms of the two sub-phases are also synchronous and sinusoidal. When the two sub-phases are connected in series, the proposed machine can also work well as a traditional PM machine. The combined EMF waveforms are given in Fig. 4 (c), which are even more sinusoidal than the individual EMF waveforms of each sub-phase. The EMF harmonics of each sub-phase winding and the combined winding are given in Fig. 4 (d), and one can find that all the EMFs have almost the same harmonic components. The magnitude of the fundamental components in the EMFs of the sub-phase windings are almost equal, the sum of which is almost equal to the magnitude of the fundamental EMF component of the combined winding.

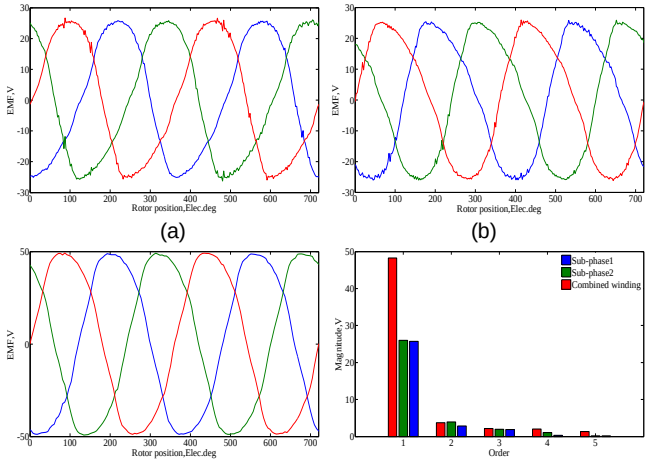

Fig. 4. Back EMF at 800 rpm when rotor PMs are removed. (a) Sub-phase 1. (b) Sub-phase 2. (c) Combined winding. (d) Harmonics.

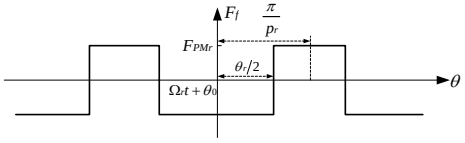

Fig.5. Air-gap MMF produced by rotor PMs.

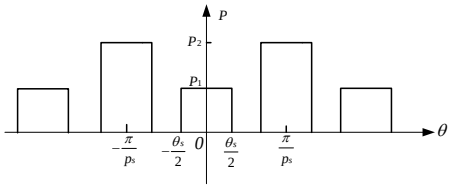

Fig.6. Air-gap permeance model of stator.

B. Rotor-PM magnetic geared machine

When the stator PMs are removed, the proposed machine can be regarded as a rotor-PM magnetic geared machine. The magnetic field excited by the rotor PMs is modulated by the stator teeth, and then couples with the armature field to produce steady electromagnetic torque. The MMF of the rotor PMs is assumed to be square wave with air-gap circumferential position θ, as shown in Fig. 5. The Fourier series expansion $F_{PMr}(\theta,t)$ is given by [34]

$$F_{PMr}(\theta,t) = \sum_{k=1}^{\infty} \frac{-4F_{PMr}}{k\pi} \sin kp_r \frac{\theta_r}{2} \cos kp_r(\theta - \Omega_r t - \theta_0) \tag{5}$$

in which, F_{PMr} refers to the value of rotor-PM MMF, Ω_r is the angular speed of the rotor, θ_r and θ_0 are the rotor pole arc and

the initial rotor position, respectively. The air-gap permeance model of stator is presented in Fig. 6, and its Fourier series is given by

$$P_s(\theta)=\frac{P_1+P_2}{2}-\sum_{n=1,3,5...}^{\infty}\frac{2(P_2-P_1)}{n\pi}\sin np_s\frac{\theta_s}{2}\cos np_s\theta \tag{6}$$

where P_1 and P_2 are the value of stator permeance corresponding to the position of stator PM and stator tooth, θ_s refers to the arc of stator tooth which is equal to the arc of the stator PM. The magnetic field excited by the rotor PMs $B_{PMr}(\theta,t)$ can be obtained by multiplying $F_{PMr}(\theta,t)$ and $P_s(\theta)$

$$\begin{cases} B_{PMr}(\theta,t)=F_{PMr}(\theta,t)P_s(\theta) \\ =-\dfrac{4F_{PMr}(P_1+P_2)}{\pi}\sum_{k=1}^{\infty}B_k\cos kp_r(\theta-\Omega_r t-\theta_0) \\ +\dfrac{4F_{PMr}(P_2-P_1)}{\pi^2}\sum_{n=1,3,5...}^{\infty}\sum_{k=1}^{\infty}A_nB_k(\cos\alpha_1+\cos\alpha_2) \\ \alpha_1=(np_s+kp_r)\left[\theta-\dfrac{kp_r(\Omega_r t+\theta_0)}{np_s+kp_r}\right] \\ \alpha_2=(np_s-kp_r)\left[\theta+\dfrac{kp_r(\Omega_r t+\theta_0)}{np_s-kp_r}\right] \\ A_n=\dfrac{1}{n}\sin\left(np_s\dfrac{\theta_s}{2}\right),B_k=\dfrac{1}{k}\sin\left(kp_r\dfrac{\theta_r}{2}\right) \end{cases} \tag{7}$$

From Eq. (7), one can find that there are three groups contained in the rotor PM harmonics. The first item is the original harmonics of the rotor PMs, with kp_r pole-pairs and rotate synchronously with the rotor. The second and the third items are np_s+kp_r and np_s-kp_r pole-pair harmonics, corresponding to α_1 and α_2 in Eq. (7), respectively. According to Eq. (2) and (3), the third items in Eq. (7) have the same pole pairs and are synchronous with the armature field when $n=1,k=1$. Consequently, steady electromagnetic torque is generated.

For the rotor-PM magnetic geared machine, the DC bias current can also act as the air-gap field regulator, since the flux generated by the DC bias current shares the same magnetic path with the stator PMs, and the pole-pair number is equal to that of stator PMs. When the field excited by DC bias current is modulated by the rotor, the harmonics with np_s+kp_r and np_s-kp_r pole-pairs are generated, which are synchronous with the second and third group of harmonic items in Eq. (7), respectively. Therefore, the magnetic field excited by the rotor PMs can also be regulated by controlling the DC bias current.

IV. Control Strategy

The whole stator winding is divided into two sub-phases and separately controlled. The overall control block diagram is shown in Fig. 7. The d-axis reference current is set to zero during the control process. The AC component is totally transformed to q-axis current to produce electromagnetic torque, while the DC bias current is transformed to zero sequence current to regulate flux. The Clarke transformer and Park transformer for the proposed machine can be expressed as

$$\begin{bmatrix} i_{\alpha1} \\ i_{\beta1} \\ i_{\alpha\beta01} \\ i_{\alpha2} \\ i_{\beta2} \\ i_{\alpha\beta02} \end{bmatrix}=\sqrt{\frac{2}{3}}\begin{bmatrix} 1 & -\frac{1}{2} & -\frac{1}{2} & 0 & 0 & 0 \\ 0 & \frac{\sqrt{3}}{2} & -\frac{\sqrt{3}}{2} & 0 & 0 & 0 \\ \frac{1}{\sqrt{2}} & \frac{1}{\sqrt{2}} & \frac{1}{\sqrt{2}} & 0 & 0 & 0 \\ 0 & 0 & 0 & 1 & -\frac{1}{2} & -\frac{1}{2} \\ 0 & 0 & 0 & 0 & \frac{\sqrt{3}}{2} & -\frac{\sqrt{3}}{2} \\ 0 & 0 & 0 & \frac{1}{\sqrt{2}} & \frac{1}{\sqrt{2}} & \frac{1}{\sqrt{2}} \end{bmatrix}\begin{bmatrix} i_{A1} \\ i_{B1} \\ i_{C1} \\ i_{A2} \\ i_{B2} \\ i_{C2} \end{bmatrix} \tag{8}$$

$$\begin{bmatrix} i_{d1} \\ i_{q1} \\ i_{01} \\ i_{d2} \\ i_{q2} \\ i_{02} \end{bmatrix}=\begin{bmatrix} \cos\theta & -\sin\theta & 0 & 0 & 0 & 0 \\ \sin\theta & \cos\theta & 0 & 0 & 0 & 0 \\ 0 & 0 & 1 & 0 & 0 & 0 \\ 0 & 0 & 0 & \cos\theta & -\sin\theta & 0 \\ 0 & 0 & 0 & \sin\theta & \cos\theta & 0 \\ 0 & 0 & 0 & 0 & 0 & 1 \end{bmatrix}\begin{bmatrix} i_{\alpha1} \\ i_{\beta1} \\ i_{\alpha\beta01} \\ i_{\alpha2} \\ i_{\beta2} \\ i_{\alpha\beta02} \end{bmatrix} \tag{9}$$

By substituting Eq. (1) into Eq. (8), the zero-sequence current i_0 can be obtained, as followed.

$$\begin{cases} i_{01}=\sqrt{3}I_{dc} \\ i_{02}=-\sqrt{3}I_{dc} \end{cases} \tag{10}$$

From Eq. (10), the zero-sequence current i_0 is proportional to the DC bias current I_{dc}, so the control of I_{dc} can be realized by controlling i_0, as shown in Fig. 7.

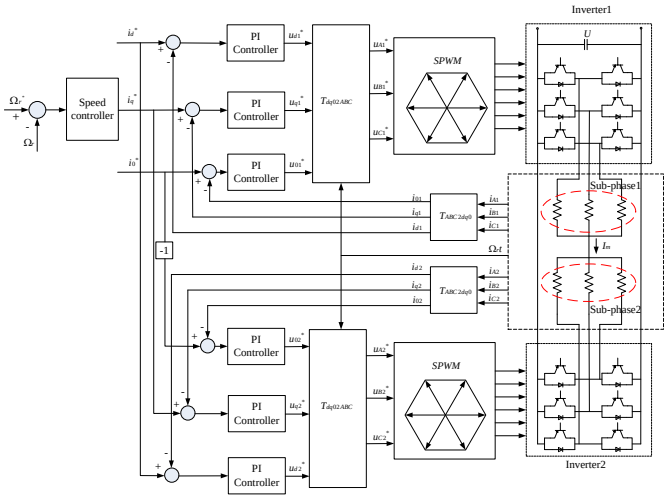

Fig. 7. Control block diagram of the proposed machine.

PI controllers are used to regulate the dq0-axis currents to reach their reference values. Detailed design method of PI controllers including how to select the gains are reported in [35]. Since the temperature rise is greatly influenced by the copper loss, the total copper loss needs to be kept constant during the flux regulating process. The equivalent current I_e is defined and expressed in Eq. (11), when DC bias current is applied, the value of AC component is subsequently reduced to keep the equivalent current I_e unchanged, so the copper loss is unchanged.

$$I_e=\sqrt{\frac{1}{T}\int_0^T\left[I_{ac}\cos(2\pi ft)+I_{dc}\right]^2dt}=\sqrt{\frac{I_{ac}^2}{2}+I_{dc}^2} \tag{11}$$

A. Generating the DC bias current

The key feature of the proposed machine is the utilization of DC bias current to achieve air-gap field regulation. The stator winding is divided into two sub-phases. Sub-phase 1 is supplied by sinusoidal AC current with positive DC bias, while sub-phase 2 is supplied by sinusoidal current with negative DC bias. For traditional star-connected three-phase winding, the sinusoidal current is produced by pulse width modulation (PWM) scheme, as shown in Fig. 8 (a). Since the used inverter is voltage fed, a DC bias voltage is generated first to produce a DC bias current. The PI controller responsible to minimize the error $i_0^* - i_{01}$, and generate DC voltages which are added to reference voltage vector used for SPWM. To generate sinusoidal current with positive DC bias, the turn-on period is extended with the same value for all the pulses, as shown in Fig. 8 (b), while, to create sinusoidal current with negative DC bias, the turn-on period for all the pulses are shortened with the same value, as shown in Fig. 8 (c). The area of the shadow parts in the left figures and the corresponding right figures are equal based on the area equivalence principle.

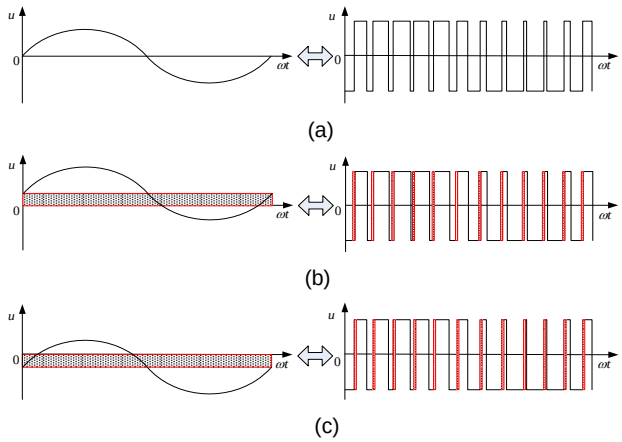

Fig. 8. PWM scheme with/without DC bias. (a) Conventional sinusoidal wave. (b) Sinusoidal wave with positive DC bias. (c) Sinusoidal wave with negative DC bias.

B. Flux weakening operation

For traditional HEMs, the armature windings and field windings are separately controlled. The armature current is used as q-axis current to produce electromagnetic torque, while the flux weakening is achieved by applying DC current to the field windings. The maximum flux weakening current can be expressed as

$$I_{HEM} = A_{slot} K_{slot} J \frac{N_{dc}}{N_{dc} + N_{ac}} \tag{12}$$

in which, J is the current density, A_{slot} and K_{slot} are the slot area and slot filling factor, respectively, while N_{ac} and N_{dc} represent the turns of armature winding and field winding, respectively. However, for the proposed machine, the maximum flux weakening current can be increased as the armature winding and field winding are integrated into one set of winding. Theoretically, the maximum flux weakening current is given in Eq. (13) with AC component equal to zero, which means all the current are used as zero sequence current to regulate the flux.

$$I_{pro} = A_{slot} K_{slot} J \tag{13}$$

The voltage equation in dq0 frame can be expressed as

$$\begin{bmatrix} u_d \\ u_q \\ u_0 \end{bmatrix} = R_s \begin{bmatrix} i_d \\ i_q \\ i_0 \end{bmatrix} + \begin{bmatrix} L_d & 0 & 0 \\ 0 & L_q & 0 \\ 0 & 0 & L_0 \end{bmatrix} p \begin{bmatrix} i_d \\ i_q \\ i_0 \end{bmatrix} + \Omega_r \begin{bmatrix} 0 & -L_q & 0 \\ L_d & 0 & 0 \\ 0 & 0 & 0 \end{bmatrix} \begin{bmatrix} i_d \\ i_q \\ i_0 \end{bmatrix} + \Omega_r \psi_f \begin{bmatrix} 0 \\ 1 \\ 0 \end{bmatrix} \tag{14}$$

where p is differential operator, R_s is the resistance of each phase, ψ_f is the excitation flux, $u_{d,q,0}$, $i_{d,q,0}$ and $L_{d,q,0}$ are the voltage, current and self-inductance in dq0 axis, respectively. If flux weakening is required, it can be achieved by adjusting the zero sequence current after i_d is set to zero. During steady condition, the differential of current is zero and the voltage equation can be rewritten as

$$\begin{aligned} u_d &= 0 \\ u_q &= R_s i_q + \omega \psi_f \\ u_0 &= R_s i_0 \end{aligned} \tag{15}$$

therefore the voltage from the inverter can be expressed as

$$u = \sqrt{u_q^2 + u_0^2} = \sqrt{\left(R_s i_q + \Omega_r \psi_f\right)^2 + \left(R_s i_0\right)^2} \tag{16}$$

One can find that the zero sequence current only involves a small voltage drop since the resistance R_s is usually very small. The i_q^* is obtained from the speed controller, which is exactly the same as the control in traditional permanent magnet synchronous machines, and i_0^* is obtained through

$$i_0^* = \frac{\sqrt{u_{\lim}^2 - \left(R_s i_q^* + \Omega_r \psi_f\right)^2}}{R_s} \tag{17}$$

where $u_{\lim}$ is the voltage limit of inverter.

C. Constant torque operation

When the proposed machine runs below the base speed and no flux regulation is required, the zero sequence current is set to zero. It means there is no DC bias in the excitation currents, and all the AC current is transformed into the q-axis current. For traditional HEMs, since the field winding is not excited and useless during constant torque operation, the maximum output torque can be expressed as

$$T_{HEM} = p \psi_f A_{slot} K_{slot} J \frac{N_{ac}}{N_{dc} + N_{ac}} \tag{18}$$

in which p is the pole-pair number, ψ_f is the flux linkage produced by the PMs. For this proposed machine, since all the windings are excited as q-axis current to produce electromagnetic torque, the maximum output torque is improved, which can be expressed as

$$T_{pro} = p \psi_f A_{slot} K_{slot} J \tag{19}$$

V. Design Considerations And Performance Analysis

A. Design considerations

Since there are various combinations of the stator and rotor pole-pair numbers for the proposed design, one of the preliminary work is to choose the most feasible $p_a / p_s / p_r$ combination for better torque performance. As higher armature frequency indicates increased iron loss, machines with small rotor pole-pairs are more preferable to reduce their armature frequency according to Eq. (3). On the other hand, machines with small stator/rotor PM number are more likely to have large cogging torque. To realize the tradeoff between low iron loss

and small cogging torque, the stator is designed with 12 slots. The possible $p_a / p_s / p_r$ combinations can be 5/6/11 and 7/6/13. The average electromagnetic torque and torque ripple rate, defined as the ratio of torque ripple peak to peak value to average torque, are simulated and compared in Fig. 9, in which the RMS value of AC current is 2A while the DC bias current is zero. One can find that the 5/6/11 pole-pair combination has larger output torque and lower torque ripple rate. Therefore, 5/6/11 pole-pair combination is used in the proposed design.

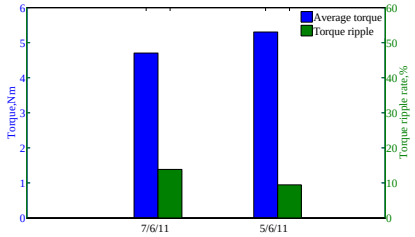

Fig. 9. Torque performance versus pole-pair combination.

The influence of the stator tooth width, rotor PM ratio (defined as the ratio of rotor PM arc to rotor pole arc) and the thickness of stator PMs as well as rotor PMs on the torque capability and no load EMF are simulated, as shown in Fig. 10. One can find that the maximum torque capability can be obtained when the rotor PM ratio is 0.6. When the stator tooth width increases, the output torque becomes slightly higher because increasing stator tooth width can increase PM flux. For the proposed machine, the stator tooth width is set to 5.8 mm. Meanwhile, when the thickness of rotor PMs and stator PMs increase, the output torque increases as well. The torque curve becomes flat when the PMs are thick enough. In this proposed design, the thickness of stator PMs and rotor PMs are 2 mm and 3 mm, respectively. The air-gap is the key component to achieve electromechanical energy conversion. Increasing the air-gap length will increase the reluctance of the magnetic path, while small air-gap length increases the assembly difficulty. In this proposed design, the air-gap length is 0.6mm.

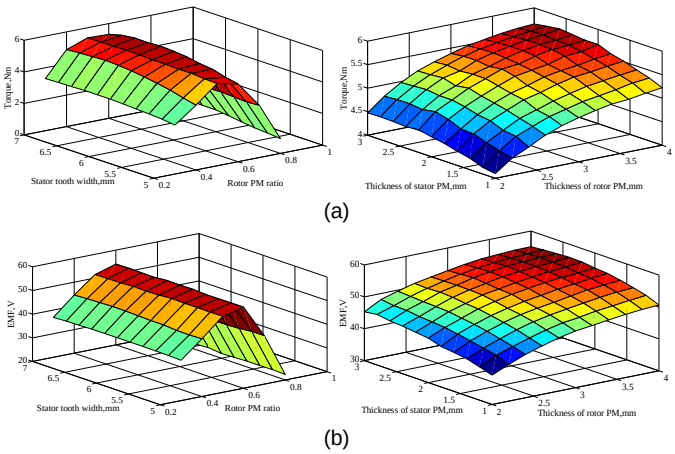

Fig. 10. Design optimization. (a) Torque. (b) No load EMF.

B. Finite element analysis

The electromagnetic performances of the proposed machine are investigated through FEA. Maxwell software package is utilized for FEM analysis. The detailed design parameters are given in Table I. In this proposed machine, there are three excitation sources, namely the rotor PMs, the stator PMs and the DC bias current. The magnetic fields excited by PMs are fixed, while the DC bias current acts as the field regulator. The regulating effect of the DC bias current to the magnetic fields excited by the two sets of PMs are separately investigated as shown in Fig. 11.

One can find that the magnetic fields excited by the stator PMs and the rotor PMs can be effectively regulated via the DC bias current. Both flux strengthening and flux weakening can be achieved by reversing the polarity of the DC bias current. For the field excited by the stator PMs, the regulating effect is more significant since the flux excited by the DC bias current and that from the stator PMs share the same magnetic path. The original harmonics with 6 pole pairs and 18 pole pairs as well as the newly emerged harmonics with 5 pole pairs, 7 pole pairs and 17 pole pairs due to the modulation of rotor are all effectively regulated by the DC bias current. Other high-order harmonics with even smaller amplitude are ignored. For the field excited by the rotor PMs, similar phenomenon can be observed. The harmonics with 5 pole pairs and 17 pole pairs due to the modulation of stator are effectively regulated.

TABLE I
DESIGN PARAMETERS

Stator outside diameter	90 mm
Stator inside diameter	57 mm
Rotor outside diameter	56 mm
Rotor inside diameter	30 mm
Length of air-gap	0.5 mm
Stack length	80 mm
Thickness of stator PMs	2 mm
Thickness of rotor PMs	3 mm
Width of stator tooth/PMs	5.8mm
Ratio of rotor PMs	0.6
Number of stator PM pole-pairs	6
Number of rotor PM pole-pairs	11
Number of armature field pole-pairs	5
Number of stator slots	12
Number of phases	3
Turns of conductors	160
Slot filling factor	65%
Current density	6.5A/mm^2
Remanence of NdFeB	1.1T
Relative permeability of NdFeB	1.05

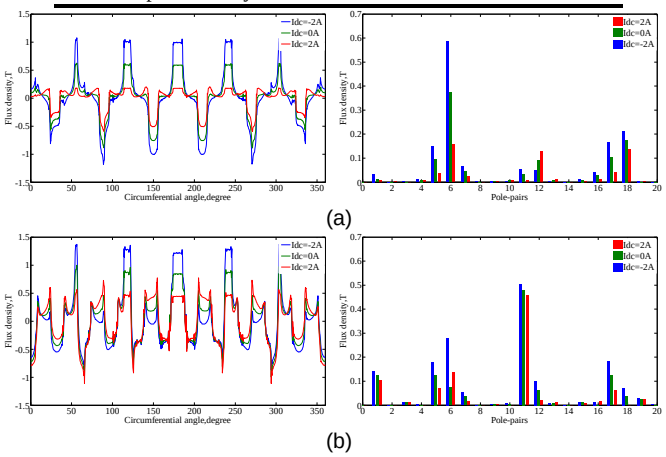

Fig. 11. Field distributions and harmonic spectrums in the air-gap. (a) Field excited by stator PMs. (b) Field excited by rotor PMs.

As the stator winding is concentrated, MMF harmonics exist

in the stator slots. The MMF waveforms produced by each phase current are given in Fig. 12. The Fourier series expansion of each phase MMF is given by

$$\begin{cases} F_a(\theta)=\sum\limits_{n=1,3,5...}^{\infty} k\dfrac{N_{ac}i_a}{n\pi}\sin\left(\dfrac{np_s\theta_s}{12}\right)\sin\left(n\dfrac{p_s}{6}\theta\right) \\ F_b(\theta)=\sum\limits_{n=1,3,5...}^{\infty} k\dfrac{N_{ac}i_b}{n\pi}\sin\left(\dfrac{np_s\theta_s}{12}\right)\sin\left[n\left(\dfrac{p_s}{6}\theta-\dfrac{2\pi}{3}\right)\right] \\ F_c(\theta)=\sum\limits_{n=1,3,5...}^{\infty} k\dfrac{N_{ac}i_c}{n\pi}\sin\left(\dfrac{np_s\theta_s}{12}\right)\sin\left[n\left(\dfrac{p_s}{6}\theta-\dfrac{4\pi}{3}\right)\right] \\ k=\begin{cases} 4\left(\dfrac{\sqrt{3}}{2}-1\right) & n=4m+1,\quad m=0,1,2... \\ 4 & n=4m+3,\quad m=0,1,2... \end{cases} \end{cases} \tag{20}$$

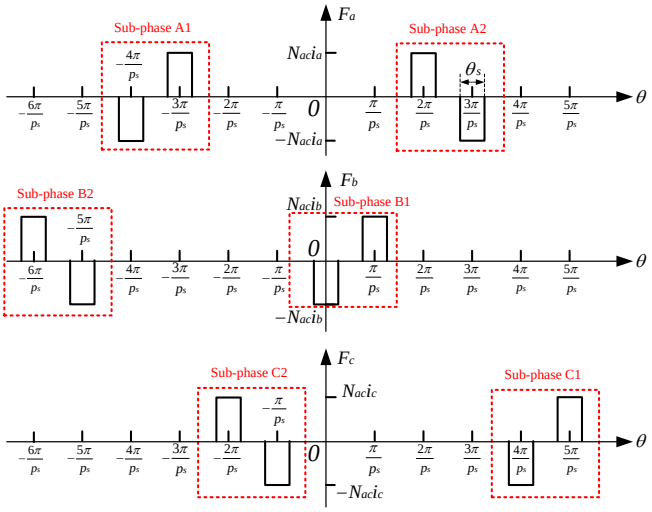

Fig.12. Air-gap MMF produced by the AC components of stator current.

in which, i_a, i_b and i_c are the AC current of each phase, respectively. N_{ac} refers to the turns of each coil. The complete MMF in the air-gap excited by the armature currents can be obtained by spatially combining the MMF waveforms of all the phase windings, as given below

$$\begin{cases} F_{ac}(\theta,t)=\sum\limits_{j=1,5,7...}^{\infty}\dfrac{3}{2}C_j\sin\left(j\dfrac{p_s}{6}\theta-h(2\pi f)t\right) \\ C_j=k\dfrac{N_{ac}I_{ac}}{j\pi}\sin\left(\dfrac{jp_s}{12}\theta_s\right) \\ h=\begin{cases} 1 & j=6i+1,\quad i=0,1,2... \\ -1 & j=6i-1,\quad i=0,1,2... \end{cases} \end{cases} \tag{21}$$

One can find that the pole-pair number of the stator MMF contains 1,5,7,11,13,17 and 19, etc. To further investigate these harmonics, the magnetic field and harmonic spectrum excited by the armature currents are given in Fig. 13. Clearly, the harmonic pole-pair matches well with the results shown in Eq. (21). The magnitude of the 5th order harmonic and the 7th order harmonic are significantly larger than that of other harmonics. Therefore, the pole-pair number of the fundamental harmonic can be chosen as 5 or 7, as described in Section V-A. The magnitude of the 5th pole-pair harmonic is even greater than that of the 7th pole-pair harmonic, that is the reason why the 5/6/11 pole-pair combination can achieve higher output torque than the 7/6/13 pole-pair combination, as shown in Fig. 9.

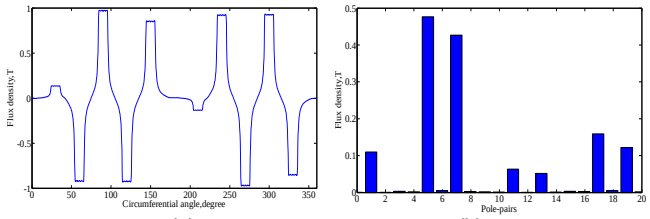

(a) (b)

Fig. 13. Field distribution and harmonics excited by armature current. (a) Field distribution. (b) Harmonic spectrum.

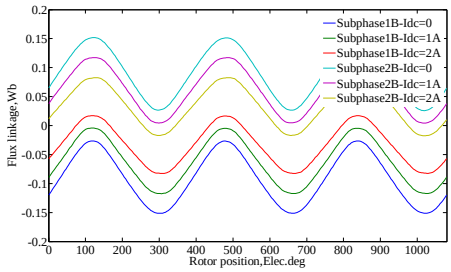

Fig. 14. Flux linkage of phase B with/without DC bias.

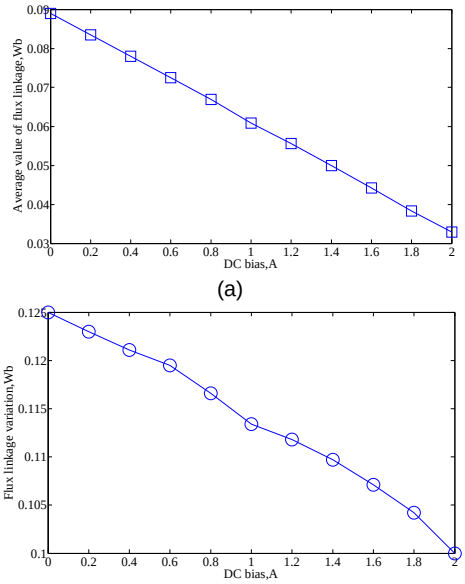

(a)

(b)

Fig. 15. Average value and variation of flux linkage when applied with different DC bias currents. (a) Average value. (b) Variation.

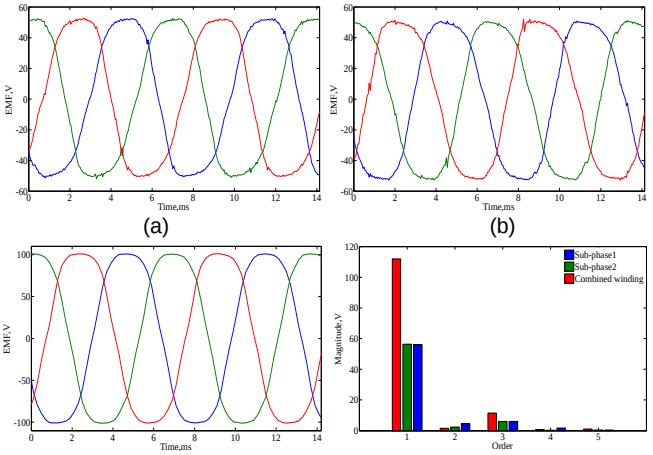

(a) (b)

(c) (d)

Fig. 16. Back EMF at 800 rpm of the proposed machine. (a) Sub-phase 1. (b) Sub-phase 2. (c) Combined winding. (d) Harmonics.

Fig. 14 shows the flux linkage of phase B with different DC bias currents. One can find that the flux linkage of sub-phase 1 and sub-phase 2 are totally synchronous. DC components can be observed in the flux linkage of both sub-phase 1 and sub-phase 2, with the same magnitude but opposite direction. Through applying positive DC bias current, both the average value and variation of the flux linkage can be weakened. Fig. 15 (a) shows the average value of the flux linkage when applied with different DC bias currents. One can see that the average value of the flux linkage decreases linearly with the increase of DC bias current. The variation of flux linkage is given in Fig. 15 (b). It can be observed that with the increasing of DC bias current, the variation of flux linkage decreases accordingly. As a result, the back-EMF is weakened. The no-load back EMF of each sub-phase and their harmonic spectrums at 800 rpm are given in Fig. 16. Balanced sinusoidal back EMFs can be obtained for both the sub-phase windings and the combined winding. Fig. 17(a) shows the torque angle characteristics with only stator-PM excitation, only rotor-PM excitation and both stator and rotor PM excitations. The RMS value of the AC current is 2 A, and the DC bias current is set to zero. One can find that both the rotor PMs and the stator PMs can interact with the armature field to produce effective electromagnetic torque. The torque capability of the proposed machine is improved. The steady state torque waveform is given in Fig. 17(b). The average torque and torque ripple are 5.3 Nm and 0.5 Nm, respectively, the torque ripple rate is acceptable. The iron loss is calculated using FEM, as shown in Fig. 18 [36].

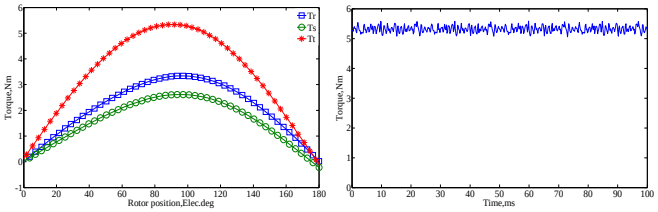

(a) (b)

Fig. 17. Torque characteristics. (a) Torque angle waveform. (b) Steady torque waveform.

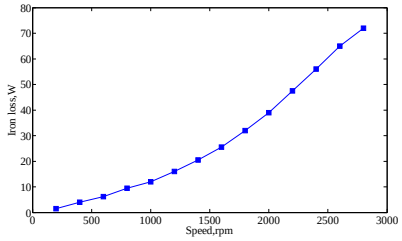

Fig. 18.Iron loss waveform.

A full-scale motor with high power is analyzed using finite element method, which is applicable for four-wheel independent-drive EV propulsion, and each wheel is employed with a motor. The outside diameter and axial length of this high power motor are 240mm and 120mm, respectively. The torque angle waveform and steady state electromagnetic torque are simulated and shown in Fig. 19. The rated torque is 158Nm when the current density is 7A/mm^2, and the rated power is 13kW. The peak torque and peak power are 384Nm and 32kW when the current density is 17A/mm^2 and the proposed machine is water cooled. The proposed machine is very suitable to be used as in-wheel motor because it's designed with outer rotor.

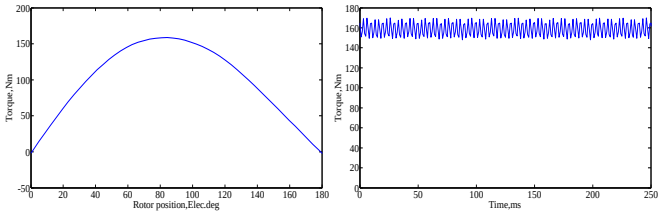

(a) (b)

Fig. 19.Torque characteristics of a full-scale high power motor. (a) Torque angle waveform. (b) Steady torque waveform.

C. Experimental verification

To verify the validity of the proposed design, a prototype with the parameters in Table I is manufactured and tested, as shown in Fig. 20. The experimental platform is established as shown in Fig. 20. The machine prototype is controlled with a floating-point DSP(TMS320F28335)-based VSI. Load torque is produced by a 1.5 kW servo machine working in generator mode and connected to its servo controller providing adjustable load torque. The experimental set up also includes a suit of torque sensor, a DC voltage source and an oscilloscope.

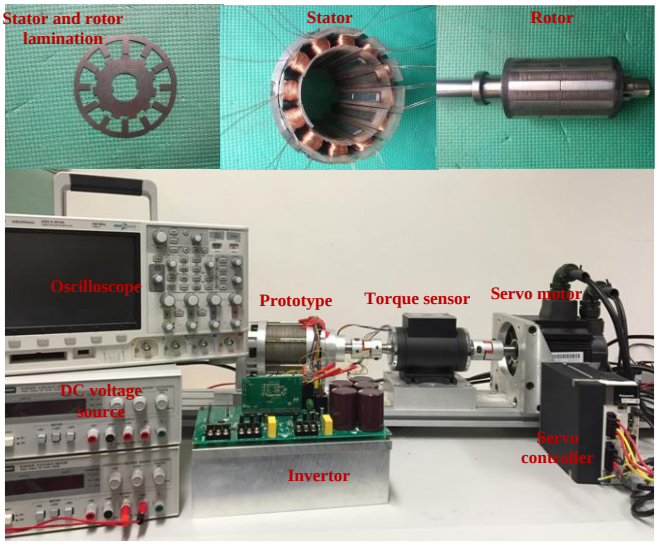

Fig. 20. Prototype and test bench.

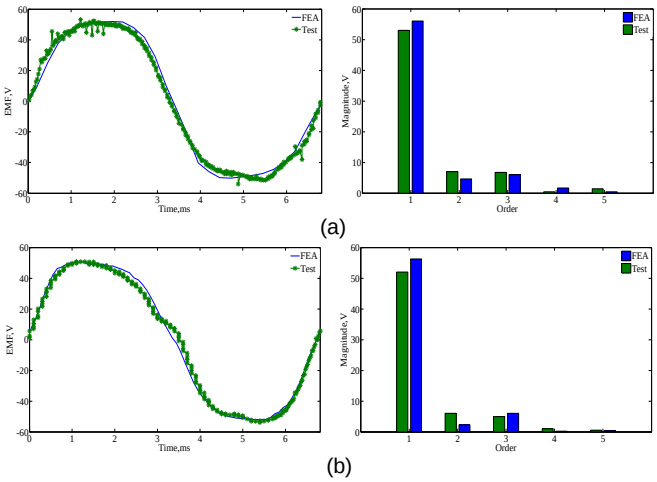

(a)

(b)

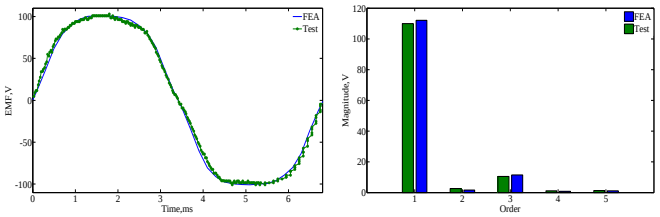

(c)

Fig. 21. Back EMF of phase A. (a) Sub-phase 1. (b) Sub-phase 2. (c) Combined winding.

Firstly, the no-load back EMFs at 800 rpm are tested and compared with the FEA results. The EMF of sub-phase A1, sub-phase A2 and combined winding as well as the harmonic spectrums are shown in Fig. 21. One can see good agreement between the results of experimental tests and FEA. Fig. 22 shows the steady state of phase current, measured torque waveform and the rotating speed of the proposed machine. Both the amplitude of the AC component and DC bias current are set to 0.35A. One can find that the excitation current of sub-phase 1 is biased by a positive offset, while the current of sub-phase 2 is biased by a negative offset. The phase currents are sinusoidal when applied with DC bias current. The corresponding torque and tested rotating speed are 0.45 Nm and 329 rpm, respectively. Fig. 23 shows the transient response of phase current, center line current I_m and rotating speed before and after applied with DC bias. The center line current is the current flows between the two sub-phases. One can see that I_m is zero when there is no DC bias in the excitation current. The current of sub-phase 1 and sub-phase 2 are almost equal with amplitude of 0.35 A. After applied with 0.6 A DC bias current, I_m increases and reaches 1.8 A, which is three times the DC bias since there are three phases in each sub-phase winding. The rotating speed of the machine also increases due to the flux weakening effect of the DC bias current. Current ripple can be observed in the center line current, because the currents of the two sub-phases are independently controlled and the control is not completely synchronized. To show the dynamic responses of the PI controllers, the currents of the two sub-phases, the center line current and the reference zero sequence current are shown in Fig. 24, in which the DC bias current is changed from 0A to 0.6A then to 0.3A and finally back to 0A. The zero sequence current i_0 is $\sqrt{3}$ times the DC bias current I_{dc}, and the center line current I_m is three times the DC bias current I_{dc}, and good dynamic response can be observed. The torque values versus different rotor positions are tested and compared with the FEA results, as shown in Fig. 25. The DC bias current is set to zero, while the RMS value of AC current is 2 A. Again, good agreement can be obtained between the results of experiment and FEA. Finally, the torque-speed and power-speed curve are tested and given in Fig. 26. One can find that the proposed machine can maintain constant power operation over a wide speed range. The efficiency is also calculated, which is 84% when the machine runs at 800 rpm and the load torque is 5 Nm. Compared with traditional PMSMs, the proposed machine has relatively lower efficiency since its magnetic gearing effect increases the reactive power and reduce the machine efficiency.

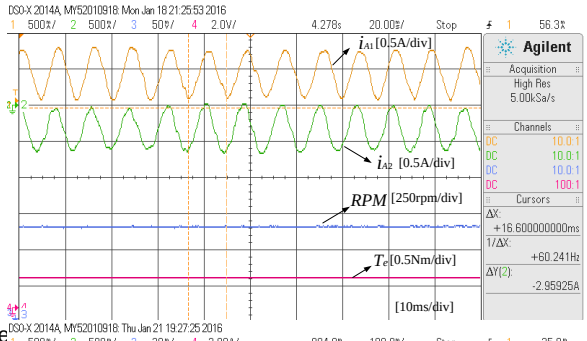

Fig. 22. Te

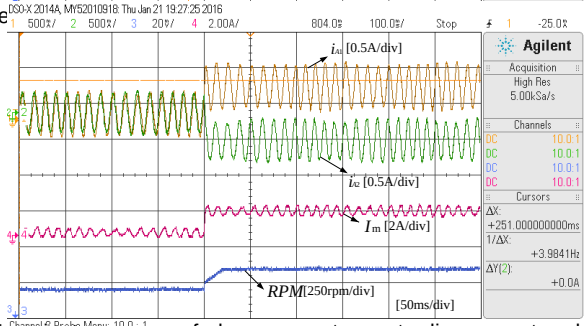

Fig. 23. Transient response of phase currents, center line current and rotating spe

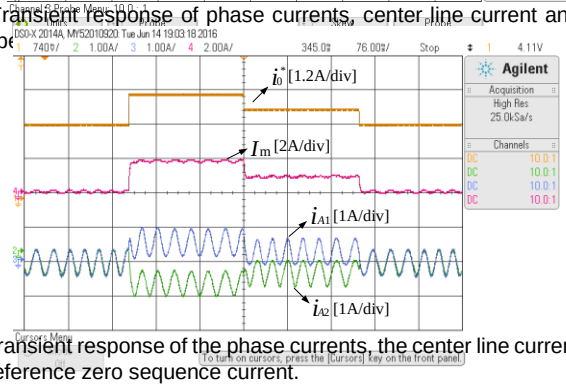

Fig. 24. Transient response of the phase currents, the center line current and the reference zero sequence current.

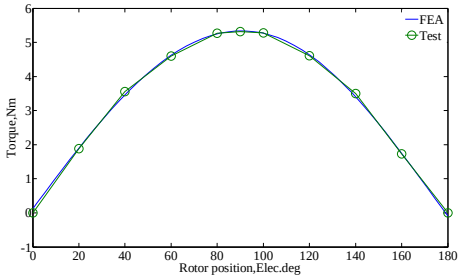

Fig. 25. Torque versus rotor position.

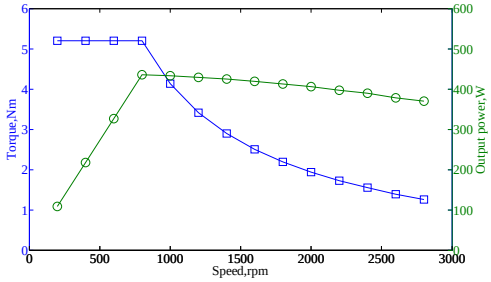

Fig. 26. Torque-speed curve and power-speed curve.

VI. Conclusion

This paper proposes a novel hybrid machine excited by AC with DC bias for EV propulsion. Dual-PM excitation is employed in the proposed design, and this machine can be regarded as the combination of a stator-PM doubly salient

machine and a rotor-PM magnetic geared machine. The torque capability of the proposed machine can be improved since both the stator PMs and the rotor PMs can contribute to the electromagnetic torque generation. The stator winding is artfully divided into two sub-phases. One is excited by sinusoidal AC current with positive DC bias, and the other is excited by sinusoidal AC current with negative DC bias, in which the DC bias current serves as a field regulator.

The machine configuration and winding connection are presented. Then the working principle of the proposed machine is investigated, in which the stator-PM doubly salient structure and the rotor-PM magnetic geared structure are separately analyzed. Control strategy is studied and the electromagnetic performances of the proposed machine are investigated by both FEA and experimental tests. The results verify that the proposed machine has good torque capability and flux regulation can be effectively achieved via DC bias current.

References

[1] S. Rivera, B. Wu, S. Kouro, V. Yaramasu, and J. C. Wang, "Electric Vehicle Charging Station Using a Neutral Point Clamped Converter With Bipolar DC Bus," *IEEE Trans. Ind. Electron.*, vol. 62, pp. 1999-2009, Apr 2015.

[2] X. H. Nian, F. Peng, and H. Zhang, "Regenerative Braking System of Electric Vehicle Driven by Brushless DC Motor," *IEEE Trans. Ind. Electron.*, vol. 61, pp. 5798-5808, Oct 2014.

[3] S. I. Kim, S. Park, T. Park, J. Cho, W. Kim, and S. Lim, "Investigation and Experimental Verification of a Novel Spoke-Type Ferrite-Magnet Motor for Electric-Vehicle Traction Drive Applications," *IEEE Trans. Ind. Electron.*, vol. 61, pp. 5763-5770, Oct 2014.

[4] Y. Gao, R. Qu, D. Li, J. Li, and G. Zhou, "Consequent-Pole Flux-Reversal Permanent-Magnet Machine for Electric Vehicle Propulsion," *IEEE Trans. Appl. Supercond.*, vol. 26, pp. 1-5, 2016.

[5] K. M. Rahman, S. Jurkovic, C. Stancu, J. Morgante, and P. J. Savagian, "Design and Performance of Electrical Propulsion System of Extended Range Electric Vehicle (EREV) Chevrolet Volt," *IEEE Trans. Ind. Appl.*, vol. 51, pp. 2479-2488, 2015.

[6] K. Rajashekara, "Present Status and Future Trends in Electric Vehicle Propulsion Technologies," *IEEE Journal of Emerging and Selected Topics in Power Electronics*, vol. 1, pp. 3-10, 2013.

[7] M. Pacas and J. Weber, "Predictive direct torque control for the PM synchronous machine," *IEEE Trans. Ind. Electron.*, vol. 52, pp. 1350-1356, Oct 2005.

[8] N. F. Lombard and M. J. Kamper, "Analysis and performance of an ironless stator axial flux PM machine," *IEEE Trans. Energy Convers.*, vol. 14, pp. 1051-1056, Dec 1999.

[9] Q. Wang and S. Niu, "Electromagnetic design and analysis of a novel fault-tolerant flux-modulated memory machine," *Energies*, vol. 8, pp. 8069-8085, 2015.

[10] Q. Wang, S. Niu, S. Ho, W. Fu, and S. Zuo, "Design and analysis of novel magnetic flux-modulated mnemonic machines," *Electric Power Applications, IET*, vol. 9, pp. 469-477, 2015.

[11] L. N. Jian, W. S. Gong, G. Q. Xu, J. N. Liang, and W. X. Zhao, "Integrated Magnetic-Geared Machine With Sandwiched Armature Stator for Low-Speed Large-Torque Applications," *IEEE Trans.Magn.*, vol. 48, pp. 4184-4187, Nov 2012.

[12] S. Pakdelian, Y. B. Deshpande, and H. A. Toliyat, "Design of an Electric Machine Integrated with Trans-Rotary Magnetic Gear," *IEEE Trans. Energy Convers.*, vol. 30, pp. 1180-1191, Sep 2015.

[13] L. Sun, M. Cheng, and H. Jia, "Analysis of a Novel Magnetic-Geared Dual-Rotor Motor With Complementary Structure," *IEEE Trans. Ind. Electron.*, vol. 62, pp. 6737-6747, Nov 2015.

[14] L. L. Wang, J. X. Shen, P. C. K. Luk, W. Z. Fei, C. F. Wang, and H. Hao, "Development of a Magnetic-Geared Permanent-Magnet Brushless Motor," *IEEE Trans.Magn.*, vol. 45, pp. 4578-4581, Oct 2009.

[15] A. Toba and T. A. Lipo, "Generic torque-maximizing design methodology of surface permanent-magnet vernier machine," *IEEE Trans. Ind. Appl.*, vol. 36, pp. 1539-1546, Nov-Dec 2000.

[16] K. Atallah, J. Rens, S. Mezani, and D. Howe, "A novel "Pseudo" direct-drive brushless permanent magnet machine," *IEEE Trans.Magn.*, vol. 44, pp. 4349-4352, 2008.

[17] Y. Liu, S. Niu, and W. Fu, "A Novel Multiphase Brushless Power-Split Transmission System for Wind Power Generation," *IEEE Trans.Magn.*, vol. 52, pp. 1-7, 2016.

[18] M. Tursini, E. Chiricozzi, and R. Petrella, "Feedforward flux-weakening control of surface-mounted permanent-magnet synchronous motors accounting for resistive voltage drop," *IEEE Trans. Ind. Electron.*, vol. 57, pp. 440-448, 2010.

[19] J. A. Tapia, F. Leonardi, and T. A. Lipo, "Consequent-pole permanent-magnet machine with extended field-weakening capability," *IEEE Trans. Ind. Appl.*, vol. 39, pp. 1704-1709, 2003.

[20] I. A. A. Afinowi, Z. Q. Zhu, Y. Guan, J. C. Mipo, and P. Farah, "Hybrid-Excited Doubly Salient Synchronous Machine With Permanent Magnets Between Adjacent Salient Stator Poles," *IEEE Trans.Magn.*, vol. 51, pp. 1-9, 2015.

[21] K. T. Chau, J. Z. Jiang, and W. Yong, "A novel stator doubly fed doubly salient permanent magnet brushless machine," *IEEE Trans.Magn.*, vol. 39, pp. 3001-3003, 2003.

[22] F. Leonardi, T. Matsuo, Y. Li, T. A. Lipo, and P. McCleer, "Design considerations and test results for a doubly salient PM motor with flux control," in *Industry Applications Conference, 1996. Thirty-First IAS Annual Meeting, IAS '96., Conference Record of the 1996 IEEE*, 1996, pp. 458-463 vol.1.

[23] X. Zhu, M. Cheng, W. Hua, J. Zhang, and W. Zhao, "Design and Analysis of a New Hybrid Excited Doubly Salient Machine Capable of Field Control," in *Industry Applications Conference, 2006. 41st IAS Annual Meeting. Conference Record of the 2006 IEEE*, 2006, pp. 2382-2389.

[24] X. Zhu, M. Cheng, W. Zhao, C. Liu, and K. T. Chau, "A Transient Cosimulation Approach to Performance Analysis of Hybrid Excited Doubly Salient Machine Considering Indirect Field-Circuit Coupling," *IEEE Trans.Magn.*, vol. 43, pp. 2558-2560, 2007.

[25] Z. Chen, B. Wang, Z. Chen, and Y. Yan, "Comparison of Flux Regulation Ability of the Hybrid Excitation Doubly Salient Machines," *IEEE Trans. Ind. Electron.*, vol. 61, pp. 3155-3166, 2014.

[26] J. T. Chen, Z. Q. Zhu, S. Iwasaki, and R. P. Deodhar, "A Novel Hybrid-Excited Switched-Flux Brushless AC Machine for EV/HEV Applications," *IEEE Trans. Veh. Technol.*, vol. 60, pp. 1365-1373, 2011.

[27] G. Zhang, W. Hua, M. Cheng, J. Liao, K. Wang, and J. Zhang, "Investigation of an Improved Hybrid-Excitation Flux-Switching Brushless Machine for HEV/EV Applications," *IEEE Trans. Ind. Appl.*, vol. 51, pp. 3791-3799, 2015.

[28] B. Gaussens, E. Hoang, M. Lecrivain, P. Manfe, and M. Gabsi, "A Hybrid-Excited Flux-Switching Machine for High-Speed DC-Alternator Applications," *IEEE Trans. Ind. Electron.*, vol. 61, pp. 2976-2989, 2014.

[29] R. L. Owen, Z. Q. Zhu, and G. W. Jewell, "Hybrid-Excited Flux-Switching Permanent-Magnet Machines With Iron Flux Bridges," *IEEE Trans.Magn.*, vol. 46, pp. 1726-1729, 2010.

[30] W. Hua, G. Zhang, and M. Cheng, "Flux-Regulation Theories and Principles of Hybrid-Excited Flux-Switching Machines," *IEEE Trans. Ind. Electron.*, vol. 62, pp. 5359-5369, 2015.

[31] Y. Wang and Z. Deng, "Comparison of Hybrid Excitation Topologies for Flux-Switching Machines," *IEEE Trans.Magn.*, vol. 48, pp. 2518-2527, 2012.

[32] H. Yang, H. Lin, Z. Q. Zhu, S. Fang, and Y. Huang, "A Dual-Consequent-Pole Vernier Memory Machine," *Energies*, vol. 9, p. 134, 2016.

[33] K. Atallah and D. Howe, "A novel high-performance magnetic gear," *IEEE Trans.Magn.*, vol. 37, pp. 2844-2846, 2001.

[34] Z. Wu and Z. Zhu, "Analysis of air-gap field modulation and magnetic gearing effects in switched flux permanent magnet machines," *IEEE Trans.Magn.*, vol. 51, pp. 1-12, 2015.

[35] K. Ogata, *Modern control engineering*: Prentice Hall PTR, 2001.

[36] D. Lin, P. Zhou, W. Fu, Z. Badics, and Z. Cendes, "A dynamic core loss model for soft ferromagnetic and power ferrite materials in transient finite element analysis," *IEEE Trans.Magn.*, vol. 40, pp. 1318-1321, 2004.

Qingsong Wang received the B.Sc. degree from the College of Automotive Engineering, Jilin University, Changchun, China, in 2012, and M.Sc. degree in the School of Automotive Studies, Tongji University, Shanghai, China, in 2015. He is currently pursuing a Ph.D. degree in the Department of Electrical Engineering at The Hong Kong Polytechnic University, Kowloon, Hong Kong.

His research interests include the design of novel electric machines, EV/HEV propulsion, and renewable energy systems.

Shuangxia Niu received the B.Sc. and M.Sc. degrees in electrical engineering from the School of Electrical Engineering and Automation, Tianjin University, Tianjin, China, in 2002 and 2005, respectively, and the Ph.D. degree in electrical engineering from the Department of Electrical and Electronic Engineering, The University of Hong Kong, Hong Kong, in 2009. Since 2009, she has been with The Hong Kong Polytechnic University, Kowloon, Hong Kong, where she is currently an Assistant Professor in the Department of Electrical Engineering. She has authored or coauthored over 60 papers in leading journals. Her research interests include the design and control of novel electrical machines and drives, renewable energy conversion systems, and applied electromagnetics.

Xiang Luo(M'16) received the B.Sc., M.Sc. and Ph.D. degrees in electrical engineering from the School of Electrical Information and Electrical Engineering, Shanghai Jiao Tong University, Shanghai, China, in 2005, 2009 and 2013, respectively.

Since 2013, he has been with The Shanghai Jiao Tong University, where he is currently a Research Associate in the School of Electrical Information and Electrical Engineering. His research interests include electrical machines, motor drives for electric vehicles, renewable energy generation and applied electromagnetics.